

Locality-aware Cross-modal Correspondence Learning for Dense Audio-Visual Events Localization

Ling Xing, Hongyu Qu, Rui Yan, Xiangbo Shu, and Jinhui Tang

Abstract—Dense-localization Audio-Visual Events (DAVE) aims to identify time boundaries and corresponding categories for events that can be heard and seen concurrently in an untrimmed video. Existing DAVE solutions extract audio and visual features through modality-specific encoders and fuse them via dense cross-attention. The independent processing of each modality neglects their complementarity, resulting in *modality-specific noise*, while dense attention fails to account for *local temporal continuity* of events, causing *irrelevant signal distractions*. In this paper, we present LoCo, a Locality-aware cross-modal Correspondence learning framework for DAVE. The core idea is to explore local temporal continuity nature of audio-visual events, which serves as informative yet free supervision signals to guide the filtering of irrelevant information and inspire the extraction of complementary multimodal information during both unimodal and cross-modal learning stages. i) Specifically, LoCo applies Locality-aware Correspondence Correction (LCC) to unimodal features via leveraging cross-modal local-correlated properties without any extra annotations. This enforces unimodal encoders to highlight similar semantics shared by audio and visual features. ii) To better aggregate such audio and visual features, we further customize Cross-modal Dynamic Perception layer (CDP) in cross-modal feature pyramid to understand local temporal patterns of audio-visual events by imposing local consistency within multimodal features in a data-driven manner. By incorporating LCC and CDP, LoCo provides solid performance gains and outperforms existing DAVE methods.

Index Terms—Audio-visual events localization, Local cross-modal coherence, Cross-modal correspondence learning

I. INTRODUCTION

In real-world scenarios, events manifest across multiple modalities, each naturally correlated with the others [2]–[10]. To enhance the perception of the world through multimodal signals, Audio-Visual Event Localization (AVEL) [11] is introduced to identify a single audio-visual event (*i.e.*, both audible and visible in video segments) in a trimmed video. This involves an unrealistic assumption that only one event occurs in a video with a short duration.

To address this limitation, we explore a more practical task, Dense-localizing Audio-Visual Events (DAVE) [12], which aims at recognizing and localizing multiple audio-visual events in a long untrimmed video. To better handle complex scenarios, DAVE allows events to overlap in time and exhibit varying durations. Both AVEL and DAVE focus on recognizing events that are audible and visible. However, the tasks differ significantly: AVEL is defined as a classification task at the

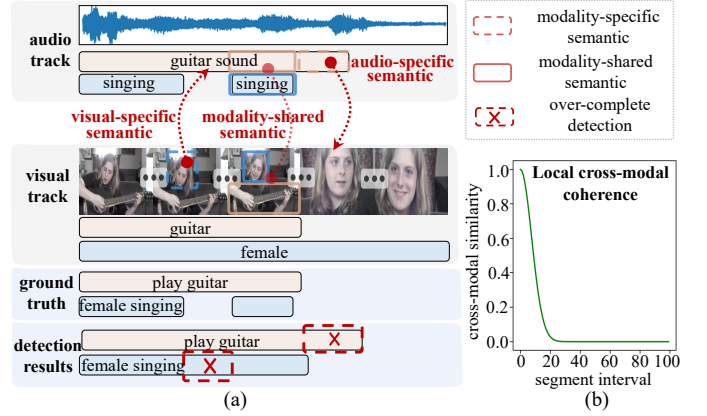


Fig. 1. (a) The diagram of over-complete detection due to modality-specific semantic interference in DAVE. When the audio track contains guitar sounds without corresponding visual evidence of guitar-playing, the model incorrectly identifies this audio-only event as an audio-visual event (“play guitar”). This misclassification highlights the vulnerability of the model to modality-specific distractions. (b) The illustration of local cross-modal coherence. Within UnAV-100 dataset and OP backbone [1], we calculate average cosine similarity between audio and visual segment features. Adjacent segments exhibit similarity, while remote segments remain distinct. Our model explicitly explores it to mine modality-shared semantics and ignore noise.

segment level [11], [13]–[15], whereas DAVE requires frame-level classification and event boundary regression to accurately localize events [12], [16]. These differences prevent the AVEL methods from being directly applicable to DAVE.

Existing DAVE solutions [12], [16] typically first extract audio and visual features through modality-specific encoders, which are then fused by dense cross-attention mechanism in a pyramid manner. Though straightforward, they have two key limitations: **First**, independent unimodal processing introduces unimodal bias, where the model may focus on modality-specific features without fully exploiting the *complementary nature of the two modalities*. This makes it vulnerable to *modality-specific distractions*, leading to inaccurate localization. As shown in Fig. 1(a), the model incorrectly classifies an audio-only guitar sound as an audio-visual event. **Second**, dense cross-attention overlooks the *local temporal continuity* of events, treating all cross-modal interactions equally and failing to prioritize locally relevant features. Hence, the model is *distorted by irrelevant signals*, such as background noise or unrelated events, compromising its ability to capture key details in long videos with complex temporal patterns.

The above discussions motivate us to propose a Locality-aware cross-modal Correspondence learning framework: LoCo, which addresses the weakness of previous attention-

L. Xing, H. Qu, R. Yan, X. Shu, and J. Tang are with the School of Computer Science and Engineering, Nanjing University of Science and Technology, Nanjing 210094, China. E-mail: {lingxing, quhongyu, ruiyan, shuxb, jinhuitang}@njust.edu.cn. (Corresponding author: Jinhui Tang)

based DAVE methods by making full use of cross-modal correlation in an elegant manner. The core idea is to explore the local temporal continuity nature of audio-visual events (*i.e.*, *local cross-modal coherence*) to boost DAVE. As shown in Fig. 1(b), close-range audio-visual segments exhibit similarity, while remote segments remain distinct. It acts as valuable yet free supervision signals that guide the filtering of irrelevant noise and inspire the extraction of complementary multimodal features during both unimodal and cross-modal learning stages.

In detail, LOCo applies **Locality-aware Correspondence Correction (LCC)** to unimodal features in the contrastive scheme, which enforces modality-specific encoders to focus on modality-shared semantics via leveraging mutual guidance between audio-visual signals, *i.e.*, cross-modal local-correlated properties. To better aggregate such semantically aligned audio and visual features, we further introduce **Cross-modal Dynamic Perception (CDP)** in multi-modal feature pyramid. CDP captures local temporal patterns of audio-visual events in the video via window-based mechanism. Different from fix-sized hand-crafted window attention [17], CDP employs Window Adaptation module to dynamically adjust attention regions in a data-driven manner. This adaptive mechanism selectively aggregates event-specific multimodal features, rather than relying on global or predefined attention regions, thereby enhancing intra-event coherence and improving the handling of videos with complex temporal structures.

It is worth mentioning that, beyond boosting the detection performance, LOCo enjoys two compelling attributes: **1 Compatibility**: LOCo is compatible with current popular transformer-based DAVE solutions, as LCC enables seamless integration of uni-modal encoders without modifications to the network architecture and CDP is closely akin to the transformer architecture maintaining consistent input and output formats. **2 Efficiency**: LOCo leverages the inherent temporal continuity of audio-visual events in video sequences, eliminating the need for extra temporal annotations. Compared to existing DAVE methods [12], [16], LOCo achieves lower FLOPs and fewer parameters (see in Tab. VII).

By incorporating LCC and CDP, LOCo automatically mines event-valuable information and filters out irrelevant noise to help precise detection with the guidance of local cross-modal coherence. We evaluate our LOCo on DAVE benchmark UnAV-100 [12]. Experiments prove that LOCo surpasses state-of-the-art competitors across different metrics, *e.g.*, **4.3%** mAP@0.9 gains on ONE-PEACE backbone [1] and **2.2%** mAP@0.5 gains on I3D-VGGish backbone [18], [19]. Furthermore, the visualization of our localization results demonstrates that, compared to the baseline, our method more effectively filters out interference from single-modal and background events, achieving more precise event localization.

Overall, our contributions are summarized as follows:

- We make the pioneering effort to leverage local cross-modal coherence for DAVE, which serves as informative yet free supervision signals to guide the extraction of event-related information from multimodal inputs during both unimodal and cross-modal learning stages.
- The proposed Locality-aware Correspondence Correction enables modality-specific encoders to learn shared cross-

modal semantics by leveraging local audio-visual correlations without requiring any manual labels.

- We devise Cross-modal Dynamic Perception to adaptively aggregate event-related multimodal features in a data-driven manner, which strengthens the grasp of local continuity patterns in audio-visual events.

II. RELATED WORK

A. Audio-Visual Event Localization

Audio-Visual Event Localization (AVEL) is to learn a model that localizes and classifies both audible and visible events, given videos and corresponding audio signals. Early AVEL approaches [11], [13]–[15] fall into the segment-level classification paradigm, highlighting action class recognition rather than precise action boundary regression. Mainstream AVEL methods can be roughly categorized into two paradigms: **i) Single-stream paradigm** [11], [20]–[23] conduct $(C + 1)$ classification at the segment level, including C audio-visual event categories and one background class. **ii) Two-stream paradigm** [13], [24]–[28] perform C -class classification at the video level to identify an audio-visual event, while simultaneously carrying out binary classification at segment level to distinguish between foreground and background. However, these methods fail to account for event-specific localization preferences, leading to unsatisfactory detection performance. To fill the gap, [15] introduces a new paradigm for localizing events, *i.e.*, event-aware localization paradigm, which leverages the localization patterns of videos within the same event category to attain better localization results. Existing AVEL methods mainly concentrate on the process of audio-visual integration. These methods [20], [21], [24], [26] all perform intra-modal temporal feature modeling and cross-modal feature interaction.

B. Dense-localizing Audio-Visual Events

AVEL methods tend to localize one audio-visual event in a short trimmed video, which is unsuitable for real-world audio-visual scenes. To address the issue, [12] proposes a more practical task (*i.e.*, Dense-localizing Audio-Visual Events (DAVE)) and corresponding benchmark (*i.e.*, UnAV-100). DAVE is a challenging task with the goal of detecting multiple audio-visual events (that may co-occur and vary in length) in a long untrimmed video. Recent works [12], [16] solely rely on modality-specific encoders to first capture intra-modal temporal relation and then learn audio-visual correspondence via the dense cross-attention mechanism in a pyramid manner to obtain multi-scale discriminative audio-visual features. However, these methods model audio-visual correspondence from a global perspective and pay less attention on unimodal learning, neglecting local inductive bias, *e.g.*, temporal prior in videos. In the image domain, existing methods [29]–[34] make use of spatial compactness to handle objects of different sizes in images. In contrast, our method accounts for the inherent characteristics of videos, *i.e.*, cross-modal temporal continuity of audio-visual video sequences, so as to better capture modality-shared information during different feature representation stages. By this means, our

framework boosts supervised learning of DAVE with cross-modal correspondence learning in a self-supervised and data-driven manner.

C. Uni-Modal Temporal Action Detection

Temporal Action Detection (TAD) aims to localize and classify all actions in an untrimmed video. Recent TAD solutions can be roughly divided into two classes: **i) Two-stage** approaches first generate action proposals through anchor windows [35], [36] or detecting action boundaries [37], [38], and then classify them into actions properly. However, they heavily rely on high-quality action proposals, hence increasing computational costs and not facilitating end-to-end training. **ii) One-stage** approaches detect all action instances in an end-to-end manner, without using any action proposal. Recent approaches attempt to localize action instances in a DETR-like [39] style, yet dense attention in the original DETR encoder relates all segments without any inductive bias, suffering from the distribution over-smoothing problem. Thus DETR-based methods [38], [40]–[42] replace standard dense attention in transformer encoder with boundary-sensitive module [41], temporal deformable attention [43], or query relation attention [42]. Apart from DETR-based solutions, another line of transformer-based works [17], [44] learn multi-level pyramid temporal representation. Though impressive, these methods only localize visible events without the help of audio modality, neglecting both audible and visible events in real-life scenes. In contrast, our focus is to Dense-localization Audio-Visual Event (DAVE) – a more challenging task that requires jointly addressing audio and visual information in an untrimmed video, facilitating audio-visual scene understanding. With respect to this, we capture discriminative multimodal features via exploring the local cross-modal coherence prior.

III. METHOD

A. Problem Statement

Dense-localizing audio-visual events (DAVE) aims to simultaneously identify the categories and instance boundaries (*i.e.*, starting and ending time) for all audio-visual events, which may overlap and vary in duration within an untrimmed video. Concretely, the input is audio-visual video sequence $\mathcal{X} = \{\{A_t\}, \{V_t\}\}_{t=1}^T$, which is represented by T audio-visual segment pairs (T differs among videos). A_t is the audio track and V_t is the visual counterpart at the t -th segment. The groundtruth audio-visual event set is expressed as $\mathcal{Y} = \{Y_n = (s_n, e_n, c_n)\}_{n=1}^N$, where N is unique to videos. The n -th audio-visual event Y_n is characterized by its starting time s_n , ending time e_n and event label $c_n \in \{0, 1\}^C$ (C represents the number of predefined categories). Note that the constraint $s_n < e_n$ must hold. The DAVE model is expected to predict $\hat{\mathcal{Y}} = \{\hat{Y}_t = (d_t^s, d_t^e, p_t)\}_{t=1}^T$, where $p_t \in \mathbb{R}^C$ denotes the probabilities for C event categories at time t , $d_t^s > 0$ and $d_t^e > 0$ refer to the distances from time t to the start and end timestamps of the event respectively. Every timestamp t in the video \mathcal{X} is a potential action candidate, while d_t^s and d_t^e are meaningful only when an event occurs at moment t . The

final audio-visual event localization results are calculated as follows:

$$\hat{s}_t = t - d_t^s, \hat{e}_t = t + d_t^e, \hat{c}_t = \arg \max p_t. \quad (1)$$

B. Overall Framework

As illustrated in Fig. 2, given audio-visual video sequence $\mathcal{X} = \{\{A_t\}, \{V_t\}\}_{t=1}^T$, our proposed LOCO is to yield precise event localization results $\hat{\mathcal{Y}}$. Formally, the proposed LOCO model is defined by:

$$\hat{\mathcal{Y}} = f_{\text{dec}}(f_{\text{enc}}(f_{\text{in}}(\{V_t\}_{t=1}^T, \{A_t\}_{t=1}^T))), \quad (2)$$

where $f_{\text{in}}(\cdot)$ is the multimodal input encoding module, $f_{\text{enc}}(\cdot)$ refers to dynamic cross-modal perception pyramid and $f_{\text{dec}}(\cdot)$ is multimodal decoder.

Multimodal Input Encoding. Following [16], we initially employ the frozen visual and audio encoders of the pre-trained model ONE-PEACE [1] to extract visual features $F_v \in \mathbb{R}^{T \times D}$ and audio features $F_a \in \mathbb{R}^{T \times D}$ respectively, where D is the feature dimension. To capture long-term temporal relations among uni-modal segments, F_v and F_a are then fed into L_u stacked uni-modal transformer blocks separately, *i.e.*, $f_v(\cdot)$ and $f_a(\cdot)$, resulting in $\hat{F}_v \in \mathbb{R}^{T \times D}$ and $\hat{F}_a \in \mathbb{R}^{T \times D}$. We propose Locality-aware Correspondence Correction (LCC, *c.f.* §III-C) to highlight modality-shared information within an audio-visual correspondence-aware contrastive learning scheme, which poses constraints on uni-modal learning stage.

Dynamic Cross-modal Perception Pyramid. The cross-modal encoder $f_{\text{enc}}(\cdot)$ aggregates complementary information from \hat{F}_v and \hat{F}_a across different temporal resolutions, to address different lengths of audio-visual events. Concretely, \hat{F}_v and \hat{F}_a are processed through L_c Cross-modal Dynamic Perception (CDP, *c.f.* §III-D) blocks with downsampling in between, producing audio-related visual feature pyramid $\mathcal{Z}_v = \{\mathcal{Z}_v^l\}_{l=1}^{L_c}$ and visual-related audio feature pyramid $\mathcal{Z}_a = \{\mathcal{Z}_a^l\}_{l=1}^{L_c}$, where $\mathcal{Z}_v^l, \mathcal{Z}_a^l \in \mathbb{R}^{T_l \times D}$ are outputs from l -th block and T_{l-1}/T_l is downsampling ratio. Multimodal feature pyramid $\mathcal{Z} = \{\mathcal{Z}^l\}_{l=1}^{L_c} \in \mathbb{R}^{T_l \times 2D}$ is then obtained by concatenating \mathcal{Z}_v and \mathcal{Z}_a at the same pyramid level. Note that, each pyramid layer is responsible for addressing events within a pre-specified time range (*e.g.*, when the downsampling ratio is 2, the third pyramid layer focuses on events spanning 8 to 16 seconds), with higher levels corresponding to longer durations. In contrast to previous methods [12], [16] that enable dense cross-attention, CDP adaptatively attends multimodal inputs to enhance intra-event integrity.

Multimodal Decoder. The multimodal decoder $f_{\text{dec}}(\cdot)$ generates the final detections based on multimodal feature pyramid $\mathcal{Y} = f_{\text{dec}}(\mathcal{Z})$. In our work, $f_{\text{dec}}(\cdot)$ initially conducts comprehensive fusion on \mathcal{Z} at each pyramid level through transformer blocks. Classification head (*Cls*) then predicts the probability of C categories at each moment across all pyramid levels. Meanwhile, class-aware regression head (*Reg*) calculates distances to the starting/ending time of the event at each moment for all categories, leading to regression output shape $\mathbb{R}^{2 \times C \times T_l}$ at each pyramid level. As in [12], *Cls* is implemented using three layers of 1D convolutions followed

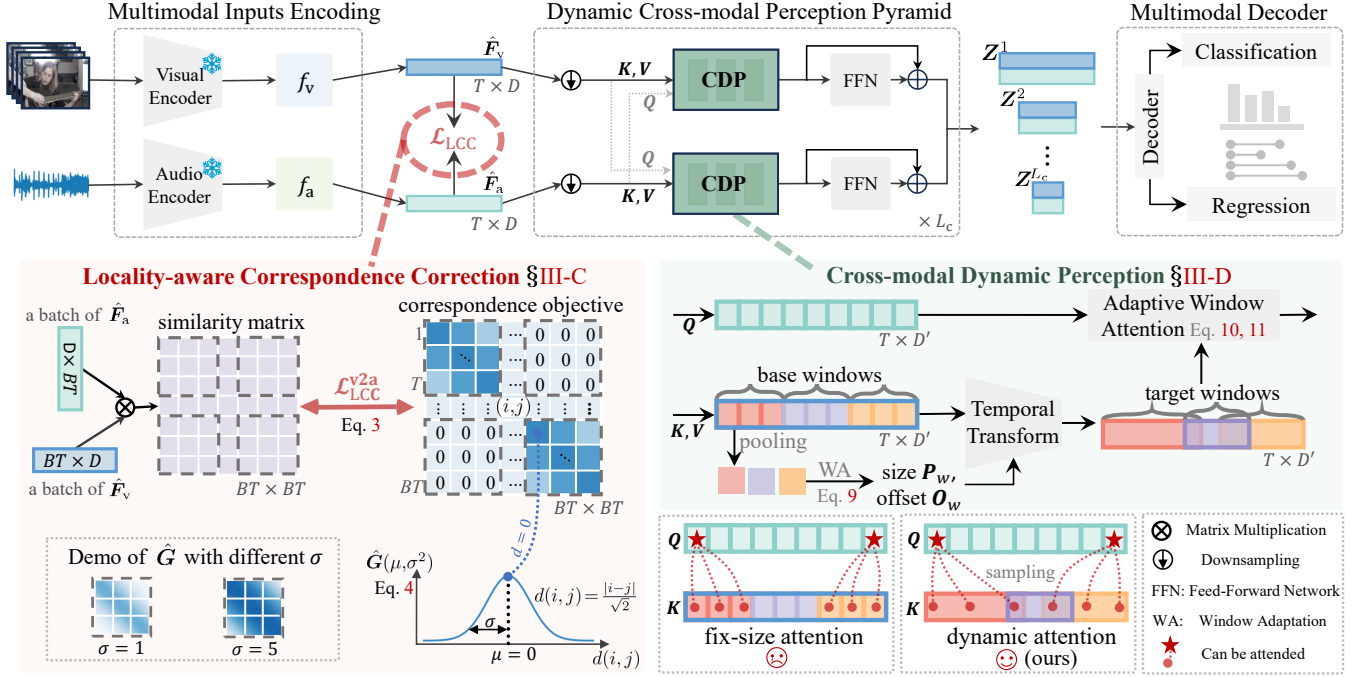


Fig. 2. **Overview of LoCo.** Visual and audio inputs are first processed by modality-specific encoders to generate initial features. Then, LoCo applies LCC to pose constraints on these initial features, emphasizing modality-shared information. Furthermore, the dynamic cross-modal perception pyramid adaptively adjusts cross-modal attention area based on inputs at all pyramid levels to enhance intra-event integrity, which consists of L_c CDP blocks and yields multimodal feature pyramid. Finally, multi-modal decoder identifies categories and time boundaries for audio-visual events.

by a sigmoid function. Reg is built with three 1D convolutions and ReLU.

C. Locality-aware Correspondence Correction

Not all of the information in complex audio-visual scenarios carries equal importance [45], [46], *e.g.*, upon hearing a dog bark, the visual area depicting the dog should be given more focus than the region of people. Thus making full use of another modality [25], [47], [48] to guide the extraction of key information (*i.e.*, modality-shared semantics) is helpful for further comprehending intricate audio-visual events. However, previous methods [11], [12], [14], [16], [22] separately encode visual and audio features without posing any cross-modal alignment constraint, disregarding temporal coherence between them. With acquired visual and audio features from multimodal input encoding modules (*i.e.*, \hat{F}_v, \hat{F}_a) in a batch, we employ LCC to pose constraints on these features, emphasizing modality-shared information. Algorithm 1 provides the pseudo-code of Locality-aware Correspondence Correction (LCC) in a PyTorch-like style.

Cross-modal Correspondence Correction. Noticing the crucial role of complementary guidance from audio and visual signals in uni-modal representation learning, we design Locality-aware Correspondence Correction (LCC) to maximize agreement between visual and audio features in the common space within a label-free contrastive learning scheme. Specifically, given audio-visual features $(\hat{F}_v, \hat{F}_a) = \{(\hat{v}_{seg}^t, \hat{a}_{seg}^t)\}_{t=1}^T$, let \mathcal{B} denotes a batch of training video features: $\mathcal{B} = \{(\hat{v}_{seg}^i, \hat{a}_{seg}^i)\}_{i=1}^M$, where $M = B \times T$ is the total number of segments in the batch (B is batch size) and

each pair $(\hat{v}_{seg}^i, \hat{a}_{seg}^i)$ corresponds to $\lceil \frac{i}{T} \rceil$ -th segment of the $[(i-1) \bmod T + 1]$ -th video features ($\lceil \cdot \rceil$ is ceiling function). Then, the contrastive loss function (to align visual modality with audio modality) is defined over \mathcal{B} as

$$\mathcal{L}_{LCC}^{v2a} = - \sum_{i=1}^M \sum_{j=1}^M \mathbf{G}_{ij} \cdot \log \frac{\exp(\langle \hat{v}_{seg}^i, \hat{a}_{seg}^j \rangle / \tau)}{\sum_{k=1}^M \exp(\langle \hat{v}_{seg}^i, \hat{a}_{seg}^k \rangle / \tau)}, \quad (3)$$

where $\tau > 0$ is a learnable temperature parameter, as in [49]. \mathbf{G}_{ij} denotes correspondence objective between \hat{v}_{seg}^i and \hat{a}_{seg}^j . Before describing the calculation of \mathbf{G} , we emphasize \mathbf{G} should ensure that values are higher for more similar pairs and 0 for negative pairs. By minimizing Eq. 3, audio-visual segment pairs within and across videos in the batch are considered, and positive pairs (*i.e.*, $\mathbf{G}_{ij} > 0$) are attracted unequally based on their similarity degree. Note that we halve the channel dimension of features to reduce computational overhead.

Prior-driven Correspondence Objective \mathbf{G} . Obtaining annotations for the similarity degree of audio-visual segment pairs for untrimmed videos is almost prohibitive, due to the difficulty in defining standardized measures of similarity. This motivates us to explore intrinsic local cross-modal coherence within a video (*i.e.*, cross-modal segment similarity decays as the segment interval increases, shown in Fig. 1(b)), which serves as a source of free supervision. Inspired by [50]–[52], the cross-modal coherence within the video can be modeled by a 2D distribution $\hat{\mathbf{G}}$, where the marginal distribution perpendicular to the diagonal follows a Gaussian distribution centered at the

Algorithm 1 Pseudo-code of Locality-aware Correspondence Correction (LCC) in a PyTorch-like style.

```

# F_v: visual features from multimodal input
  encoding modules(B, T, D)
# F_a: audio features from multimodal input
  encoding modules(B, T, D)
# B: batch size
# T: number of segments
# D: embedding dimension
# tau: a learnable temporal parameter
# sigma: a learnable standard deviation
# pi: the ratio of a circle's circumference to
  its diameter

def Calculate_LCC (F_v, F_a, tau, sigma):
  # calculate similarity matrix
  F_v = F_v.reshape(B x T, D) # (B x T, D)
  F_a = F_a.reshape(B x T, D) # (B x T, D)
  sim_v2a = F_v @ F_a.transpose(0, 1) / tau
  sim_a2v = F_a @ F_v.transpose(0, 1) / tau

  # calculate correspondence objective G (B x
    T, B x T)
  G = zeros((B x T, B x T)) # (B x T, B x T)
  for i in range(0, B x T, T):
    G_T = Gaussian(T, sigma)
    G[i : i + T, i : i + T] = G_T

  # to align visual modality with audio
    modality
  LCC_v2a = -sum(log_softmax(sim_v2a, dim=1)
    * G, dim = 1).mean()
  # to align audio modality with visual
    modality
  LCC_a2v = -sum(log_softmax(sim_a2v, dim=1)
    * G, dim = 1).mean()

  # calculate final LCC
  LCC = (LCC_v2a + LCC_a2v) / 2
  return LCC

# calculate correspondence objective within
  the same video (T, T)
def Gaussian (T, sigma):
  G_T = (arange(T).reshape(T, 1) - arange(T)
    .reshape(1, T)) / sqrt(2) # (T, T)
  G_T = - (G_T**2) / 2.0 / (sigma**2)
  G_T = 1 / (sigma * sqrt(2 * pi)) * exp(G_T)
  return G_T

```

intersection point on the diagonal, as

$$\hat{G}_{ij} = \frac{1}{\sigma\sqrt{2\pi}} \exp\left(-\frac{(d(i,j) - \mu)^2}{2\sigma^2}\right), d(i,j) = \frac{|i-j|}{\sqrt{2}}, \quad (4)$$

where μ is mean parameter, σ is standard deviation, and $d(i, j)$ measures distance between entry (i, j) and diagonal line. As shown in Fig. 2, we set $\mu=0$, ensuring synchronous audio and visual pairs are the most similar and progressively decrease perpendicular to the diagonal. A larger σ leads to broader weights, allowing pairs that are more distant from the diagonal to still receive significant attraction. Similar to τ , we set σ as a learnable parameter, facilitating the establishment of reliable cross-modal correspondence during training. Note that we treat audio-visual segment pairs from different videos (*i.e.*, $\lceil \frac{i}{T} \rceil \neq \lceil \frac{j}{T} \rceil$) as negative pairs, as in [53]–[55]. Finally, correspondence

objective G is:

$$G_{ij} = \begin{cases} \hat{G}_{ij}, & \text{if } \lceil \frac{i}{T} \rceil = \lceil \frac{j}{T} \rceil \\ 0, & \text{if } \lceil \frac{i}{T} \rceil \neq \lceil \frac{j}{T} \rceil \end{cases} \quad (5)$$

The audio-to-visual counterpart \mathcal{L}_{LCC}^{a2v} can be calculated in the same manner and LCC is applied as

$$\mathcal{L}_{LCC} = \frac{1}{2}(\mathcal{L}_{LCC}^{v2a} + \mathcal{L}_{LCC}^{a2v}). \quad (6)$$

D. Cross-modal Dynamic Perception

Core idea. As long untrimmed videos are dominated by irrelevant backgrounds, only processing valuable segments is desirable both for speed and performance, *i.e.*, ignores irrelevant contents [56], [57]. However, previous methods learn multimodal interactions by dense cross-modal attention [12], [16]. They ignore the local temporal continuity of audio-visual events in videos and introduce extra noise, leading to inaccurate detection. Thus, we devise Cross-modal Dynamic Perception (CDP) layer in cross-modal feature pyramid to reduce temporal redundancy in long videos. CDP learns adaptive attention areas in a data-driven manner and flexibly aggregates relevant multimodal features.

Base Window Construction. In Dynamic Cross-modal Perception Pyramid, CDP allows to better handle events of different durations at each pyramid level. As in Fig. 2, CDP is conducted by assigning one modality as key and value, and the other as query. We illustrate CDP with an example where audio features Z_a serve as query (visual features Z_v serve as key and value). Given Z_v^{l-1} , Z_a^{l-1} (*i.e.*, the input of l -th CDP block), downsampling is performed first to obtain $\tilde{Z}_v^l, \tilde{Z}_a^l \in \mathbb{R}^{T_l \times D}$. CDP partitions features into non-overlapping base temporal windows, *i.e.*, $\{\tilde{Z}_{v_w}^l, \tilde{Z}_{a_w}^l \in \mathbb{R}^{W \times H \times D'}\}_{w=1}^{T_l/W}$, where W is the predefined window size, H is head number and D' is channel dimension. Note that $D = H \times D'$. Specifically, given $\tilde{Z}_{a_w}^l, \tilde{Z}_{v_w}^l$, the query, key, and value features are got by:

$$Q_w^l = f_{\text{Linear}}(\tilde{Z}_{a_w}^l), \quad (7)$$

$$K_w^l, V_w^l = f_{\text{Linear}}(\tilde{Z}_{v_w}^l), \quad (8)$$

where $Q_w^l, K_w^l, V_w^l \in \mathbb{R}^{W \times H \times D'}$, and f_{Linear} is Linear layer. **Target Window Construction.** CDP applies Window Adaptation (WA) module to predict the ideal temporal sizes and offsets for each base window (*i.e.*, K_w^l, V_w^l) in a data-driven manner. WA consists of average pooling, LeakyReLU [58] activation, and 1 x 1 convolution with stride 1 in sequence:

$$P_w, O_w = f_{\text{convolution}}(f_{\text{LeakyReLU}}(f_{\text{average pooling}}(K_w^l))), \quad (9)$$

where P_w and $O_w \in \mathbb{R}^{1 \times H}$ represent the estimated temporal size and offset (V_w^l undergo the same processing). Based on P_w and O_w , each base window is transformed into target window (*i.e.*, attention area) by H attention heads independently, which differs from the method on image domain [29], [30] that window definition is shared among heads. The obtained target windows may overlap, which strengthens the ability to address overlapping events.

Adaptive Window Attention. Then CDP uniformly samples W features from all target windows over K^l, V^l respectively.

TABLE I
 QUANTITATIVE COMPARISON RESULTS (SEE §IV-C) ON UNAV-100 [12]. “ONE-PEACE” IS THE VISUAL AND AUDIO ENCODER OF ONE-PEACE [1], AND “I3D-VGGISH” DENOTES THE VISUAL ENCODER IS I3D [18] AND AUDIO ENCODER IS VGGISH [19]. THE BEST RESULTS ARE BOLD.

Method	Encoder	0.5	0.6	0.7	0.8	0.9	Avg.
VSGN [64] [ICCV2021]	I3D-VGGish	24.5	20.2	15.9	11.4	6.8	24.1
TadTR [43] [TIP2022]	I3D-VGGish	30.4	27.1	23.3	19.4	14.3	29.4
ActionFormer [17] [ECCV2022]	I3D-VGGish	43.5	39.4	33.4	27.3	17.9	42.2
TriDet [44] [CVPR2023]	I3D-VGGish	46.2	-	-	-	-	44.4
UnAV [12] [CVPR2023]	I3D-VGGish	50.6	45.8	39.8	32.4	21.1	47.8
UniAV(AT) [16] [arXiv2024]	I3D-VGGish	49.3	-	-	-	-	47.0
UniAV(STF) [16] [arXiv2024]	I3D-VGGish	50.1	-	-	-	-	48.2
ActionFormer [17] [ECCV2022]	ONE-PEACE	49.2	-	-	-	-	47.0
TriDet [44] [CVPR2023]	ONE-PEACE	49.7	-	-	-	-	47.3
UnAV [12] [CVPR2023]	ONE-PEACE	53.8	48.7	42.2	33.8	20.4	51.0
UniAV(AT) [16] [arXiv2024]	ONE-PEACE	54.1	48.6	42.1	34.3	20.5	50.7
UniAV(STF) [16] [arXiv2024]	ONE-PEACE	54.8	49.4	43.2	35.3	22.5	51.7
LoCo (Ours)	I3D-VGGish	52.8	47.6	41.1	33.3	21.9	49.5
LoCo (Ours)	ONE-PEACE	58.5	53.2	46.7	38.1	26.8	54.9

This yields $\hat{K}_w^l, \hat{V}_w^l \in \mathbb{R}^{W \times H \times D'}$ as key, value features for the query feature Q_w^l . The sampling count W is equal to base window size, which ensures computational cost remains consistent with base window attention. To bridge connections among target windows, we adopt cross-modal sliding window attention (CSWA), the process can be defined as:

$$\hat{Z}_v^l = f_{\text{CSWA}}(Q_w^l, \hat{K}_w^l, \hat{V}_w^l), \quad (10)$$

$$Z_v^l = \hat{Z}_v^l + f_{\text{FFN}}(f_{\text{LN}}(\hat{Z}_v^l)), \quad (11)$$

where $Q_w^l, \hat{K}_w^l, \hat{V}_w^l \in \mathbb{R}^{T \times H \times D'}$ are got by stacking $Q_w^l, \hat{K}_w^l, \hat{V}_w^l$ respectively. f_{LN} is LayerNorm [59] and f_{FFN} is feed-forward network [60].

Different from recent TAD method [17] exploring the local dependency in visual modality via fix-sized hand-crafted window attention, CDP dynamically adjusts the attention area based on multimodal inputs, providing a more elegant way to process complex audio-visual scenes where events can overlap and vary in duration.

E. Training and Inference

Loss Function. Following [12], [16], we employ three losses for end-to-end optimization, *i.e.*, focal loss [61] for classification \mathcal{L}_{cls} , generalized IoU loss [62] for regression \mathcal{L}_{reg} , and Locality-aware Correspondence Correction \mathcal{L}_{LCC} (*c.f.* §III-C). The total loss is calculated as:

$$\mathcal{L} = \mathcal{L}_{\text{cls}} + \mathcal{L}_{\text{reg}} + \alpha \mathcal{L}_{\text{LCC}}, \quad (12)$$

where α is 0.1 by default.

Inference. During inference, full video sequences are fed into our model to obtain event candidates. Such event candidates are further refined by multi-class Soft-NMS [63] to alleviate highly overlapping temporal boundaries within the same class.

IV. EXPERIMENTS

A. Experimental Setup

Datasets. UNAV-100 [12] is the first untrimmed audio-visual dataset, encompassing 100 classes across diverse domains (*e.g.*, human activities, music, animals, vehicles, natural sounds, and tools, *etc.*). It contains 10,790 videos, divided into training, validation, and testing sets in a 3:1:1 ratio. Each video averages 2.8 audio-visual events, annotated with categories and precise temporal boundaries.

Evaluation Metric. For evaluation, we adopt the standard metric, *i.e.*, mean average precision (mAP). The average mAP at temporal intersection over union (tIoU) thresholds [0.1:0.1:0.9] and mAPs at tIoU thresholds [0.5:0.1:0.9] are reported, as suggested by [12], [16].

B. Implementation Details

Network Architecture. As with the previous method [16], the sound sampling rate is 16 kHz, and the video frame rate is 16 FPS. The visual and audio features are extracted from the visual and audio encoders of ONE-PEACE [1], using segments of 16 frames (1s) and a stride of 4 frames (0.25s). The extracted audio and visual feature dimensions are 1536. In our model, the embedding dimension D is 512, and $L_u = 2, L_c = 6$. The initial value for the learnable standard deviation σ is 1. The head number $H = 4$. The downsampling ratio T_{l-1}/T_l in the cross-modal pyramid encoder is set to 2, which is implemented through a single depth-wise 1D convolution as in [12]. Note that features at different pyramid levels correspond to detecting the audio-visual events with different time ranges. The regression head predicts distances to the starting/ending time of the audio-visual event at each moment, where the regression range is predefined for each pyramid level, following [12], [16]. Only if the current moment lies in an audio-visual event, the regression results are valid.

To demonstrate the adaptability of our method to different video and audio backbones, we also consider I3D [18] and VGGish [19] features, used in previous works [12], [16]. Identical to [12], frames are sampled at 25 FPS for each video, with the maximum length set to 224. Then 24 consecutive RGB frames and optical flow frames (extracted by RAFT [65]) are input into the two-stream I3D model [18], using a stride of 8 frames. Meanwhile, audio features are extracted using VGGish [19] from each 0.96 seconds segment, employing a sliding window (stride = 0.32 seconds) to ensure temporal alignment with the visual features.

Training. Consistent with previous work [12], we adopt the Adam optimizer [66] with a linear warmup of 5 epochs. Specifically, we set the batch size to 16, initial learning rate to 10^{-4} and weight decay to 10^{-4} . To accommodate varying input video lengths, in the same way as [12], [16], maximum sequence length T is set to a fixed value by cropping or padding, *i.e.*, $T = 256$ for ONE-PEACE [1] features and $T = 224$ for I3D [18] and VGGish [19] features.

Reproducibility. Our model, implemented in PyTorch and python3, is trained on one RTX 3090 GPU with 24GB memory. Testing is conducted on the same machine. To guarantee reproducibility, full code will be released.

C. Comparison with State-of-the-Arts

As shown in Tab. I, LOCo adapts to different pre-trained models and consistently outperforms leading DAVE methods UnAV [12] and UniAV [16] across all metrics on the UnAV-100 [12] dataset. Concretely, equipped with the “ONE-PEACE” encoder, *i.e.*, the visual and audio encoder of ONE-PEACE [1], LOCo yields 54.9% average mAP at tIoU thresholds [0.1:0.1:0.9], while the previous state-of-the-arts method, UniAV(STF) [16], achieves a corresponding score of 51.7%. UniAV [16] is a unified audio-visual perception network, where UniAV(AT) denotes all-task model and UniAV(STF) refers to single-task model fine-tuned on UniAV(AT). Note that LOCo surpasses UniAV(STF), with **3.2%** rise in average mAP and **4.3%** boost in mAP@0.9 (*i.e.*, mAP at a tight threshold of 0.9). Utilizing the “I3D-VGGish” encoder (*i.e.*, the visual encoder is I3D [18] and the audio encoder is VGGish [19]), LOCo still surpasses existing methods in terms of mAP at different tIoU thresholds. As seen, our method LOCo obtains a **2.7%** mAP@0.5 (*i.e.*, mAP at a threshold of 0.5) gain and a 1.3% increase in average mAP, compared with UniAV(STF). Meanwhile, we compare our model LOCo with recent state-of-the-art TAL models, including two-stage model VSGN [64] and one-stage model TadTR [43], ActionFormer [17], and TriDet [44]. Consistent with [12], [16], TAL methods are provided with concatenated audio and visual features. It can be observed that our LOCo outperforms all these TAL methods by a solid margin. These results demonstrate the effectiveness of our LOCo.

D. Diagnostic Experiments

To thoroughly evaluate our model, we conduct extensive ablation studies. Firstly, we offer a detailed analysis of the key components of our method LOCo, including LCC (*c.f.* §III-C)

and CDP (*c.f.* §III-D), displayed in Tab. II and Tab. III. In addition, we compare our proposed LCC and CDP with other alternatives to confirm the advantages of these components, illustrated in Tab. IV and Tab. V respectively. We also conduct ablation experiments on key hyperparameter, *i.e.*, the base window size W in CDP, the head number H in CDP, and the weight α in Eq. 12, which are reported in Tab. VI, Fig. 4 and Fig. 5 separately. Finally, we compare our LOCo with existing state-of-the-art methods and various variants of our method regarding parameters and FLOPs, shown in Tab. VII.

Key Component Analysis based on “ONE-PEACE” Encoder. We first analyze the impact of our core designs, *i.e.*, LCC (*c.f.* §III-C) and CDP (*c.f.* §III-D) based on “ONE-PEACE” encoder [1], which are presented in Tab. II. The baseline in row #1 of Tab. II denotes our method LOCo without LCC and CDP. As shown in Tab. II, additionally considering complementary guidance from audio and visual modalities (*i.e.*, LCC) in unimodal learning stage (row #2) leads to a substantial performance gain (*i.e.*, **9.8%** mAP@0.9) compared with baseline in row #1. Besides, our model with LCC and CDP (row #4) outperforms baseline incorporating CDP (row #3) by **3.3%** in mAP@0.9 in Tab. II. Note that mAP@0.9 implies a stringent criterion for localization accuracy, underscoring the substantial improvements brought by LCC. The results indicate that LCC consistently improves performance, regardless of whether explicit cross-modal interactions (*i.e.*, CDP) are incorporated. According to row #1 and row #3 in Tab. II, CDP brings **16.6%** gains in mAP@0.9, highlighting the importance of the adaptive cross-attention strategy. In row #4 of Tab. II, LOCo with two core components together (*i.e.*, LCC and CDP) achieves the best performance, confirming the joint effectiveness of them.

TABLE II
ABLATION STUDY ON THE KEY COMPONENTS IN UNAV-100 [12] WITH THE BACKBONE ONE-PEACE [1].

LCC	CDP	0.5	0.6	0.7	0.8	0.9	Avg.
		37.1	29.0	21.6	13.6	6.9	37.0
✓		45.6	38.8	31.7	25.3	16.7	45.1
	✓	57.8	52.5	45.1	36.5	23.5	53.8
✓	✓	58.5	53.2	46.7	38.1	26.8	54.9

TABLE III
ABLATION STUDY ON THE KEY COMPONENTS IN UNAV-100 [12] WITH THE BACKBONE “I3D-VGGISH”, *i.e.*, VISUAL FEATURES EXTRACTED BY I3D [18] AND AUDIO FEATURES OBTAINED BY VGGISH [19] (SEE §IV-D).

LCC	CDP	0.5	0.6	0.7	0.8	0.9	Avg.
		34.8	27.6	19.7	10.8	3.4	33.5
✓		39.8	33.2	27.4	21.5	14.4	39.2
	✓	51.9	46.2	39.5	31.0	15.4	48.1
✓	✓	52.8	47.6	41.1	33.3	21.9	49.5

Key Component Analysis based on “I3D-VGGish” Encoder. We also study the impact of essential components of LOCo, *i.e.*, LCC (*c.f.* §III-C) and CDP (*c.f.* §III-D) based on “I3D-VGGish” encoder in Tab. III. The baseline in row #1 of Tab. III

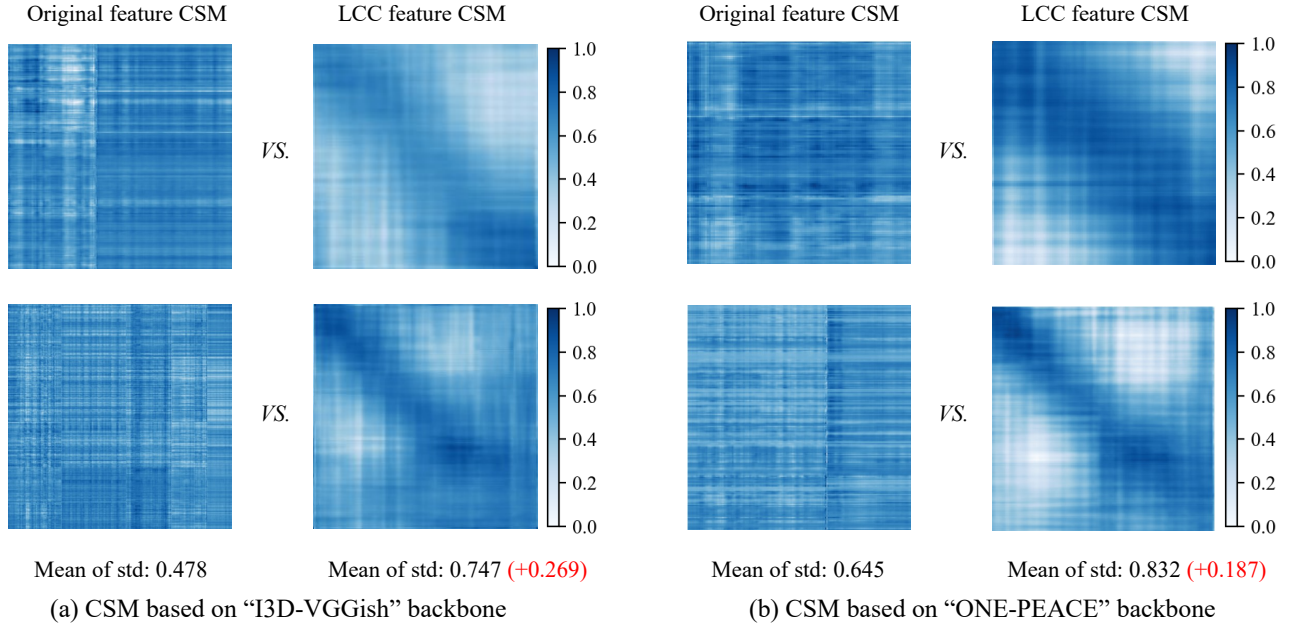


Fig. 3. **Qualitative results** show the effect of LCC (*c.f.* III-C), which increases feature discriminability. The cross-similarity matrix (CSM) is calculated between audio and visual features at different timestamps within the same video. For all videos in UnAV-100 [12] test split, the standard deviation of the CSM is calculated, and the average of them is denoted as “Mean of std”. We randomly present the CSM of two videos equipped with “I3D-VGGish” features [18], [19] and “ONE-PEACE” features [1], respectively.

denotes our method LOCo without LCC and CDP. According to Tab. III, our LOCo (row #4 of Tab. III) achieves 49.5% average mAP and 21.9% mAP@0.9, outperforming baseline (row #1 in Tab. III) by 16% in average mAP and 18.5% in mAP@0.9. By leveraging LCC to pose constraints on the uni-modal learning stage, it improves 5.0% in mAP@0.5 and 11.0% in mAP@0.9, as shown in rows #1 and #2 of Tab. III. To evaluate the effect of CDP in LOCo (*i.e.*, row #1 and row #3 in Tab. III), it shows that CDP yields a 14.6% higher average mAP than baseline. This highlights the crucial role of adaptively aggregating event-related multimodal features. Row #4 in Tab. III, *i.e.*, our full model LOCo with LCC and CDP, obtains the best performance across all metrics, which confirms the importance of the cooperation between LCC and CDP. All these results prove the effectiveness of our method with respect to the “I3D-VGGish” features.

TABLE IV
EFFECT OF CORRESPONDENCE OBJECTIVE \mathbf{G} IN EQ. 3 BASED ON
“ONE-PEACE” FEATURES [1]. (SEE §IV-D).

\mathbf{G} -type	0.5	0.6	0.7	0.8	0.9	Avg.
Diagonal matrix	57.5	52.2	46.1	37.3	25.1	53.5
Softened target	57.7	52.3	45.3	38.0	26.5	53.7
Fixed gaussian	58.0	53.1	46.5	38.0	26.2	54.4
Adjustable gaussian	58.5	53.2	46.7	38.1	26.8	54.9

Impact of Correspondence Objective \mathbf{G} in Eq. 3. By default, we use learnable gaussian distribution (*c.f.* Eq. 4), *i.e.*, “Adjustable gaussian” in row #4 of Tab. IV to calculate \mathbf{G} , where σ is a learnable parameter. As shown in Tab. IV, we evaluate three alternatives to \mathbf{G} employing “ONE-PEACE” features [1]. ① “Diagonal matrix” Λ considers only concurrent audio-visual

segment pairs as positive pairs [54], negatively impacting performance. ② “Softened target” [67] roughly employs label smoothing to relax the strict constraints imposed by diagonal matrix, *i.e.*, $\mathbf{G} = (1 - \alpha)\Lambda + \alpha/(M - 1)$, $\alpha = 0.2$. However, the equal attraction of all positive pairs hinders performance. ③ “Fixed gaussian” uses $\sigma = 1$ in Eq. 4 (*i.e.*, without adjusting σ based on input), resulting in a suboptimal solution. In terms of average mAP, LOCo with “Adjustable gaussian” outperforms LOCo with other alternatives to \mathbf{G} by a large margin, *e.g.*, “Diagonal matrix” by 1.4%, “Softened target” by 1.2%, and “Fixed gaussian” by 0.5%. We find our method surpasses all other alternatives by effectively incorporating the intrinsic, cross-modal coherence property in a data-driven manner.

TABLE V
EFFECT OF DIFFERENT ATTENTION STRATEGIES BASED ON “ONE-PEACE”
FEATURES [1] (SEE §IV-D).

Attention strategy	0.5	0.6	0.7	0.8	0.9	Avg.
Global	57.4	52.2	45.4	37.1	25.7	53.8
Fixed	57.8	52.4	45.0	37.2	26.0	53.5
Adaptive	58.5	53.2	46.7	38.1	26.8	54.9

Cross-modal Dynamic Perception. Tab. V studies the impact of Cross-modal Dynamic Perception (CDP, *c.f.* §III-D) by contrasting it with vanilla cross-attention [12] (*i.e.*, “Global”) and fixed local cross-attention (*i.e.*, “Fixed”). “Global” introduces extra noise from irrelevant backgrounds and degrades the performance compared to local attention (row #2 - #3 in Tab. V). Concretely, the average mAP of “Global” (row #1 in Tab. V) falls short of 1.1% by “Adaptive” (row #3 in Tab. V), *i.e.*, CDP. Based on our proposed CDP, we derive a variant

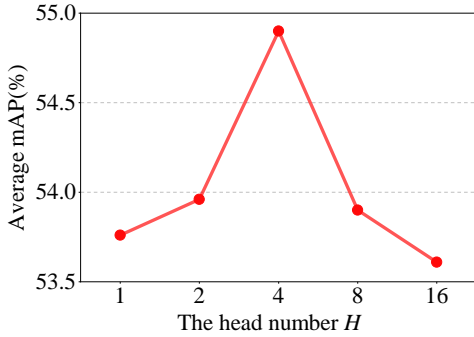


Fig. 4. **The impact of head number H** in Cross-modal Dynamic Perception (CDP) on average mAP incorporating “ONE-PEACE” backbone [1].

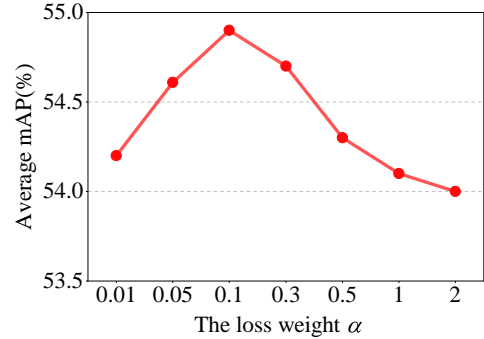


Fig. 5. **The impact of parameter α** on average mAP built upon “ONE-PEACE” features [1].

“Fixed” (row #2 in Tab. V): only realize cross-modal sliding window attention by a fixed-size window of 8 (the same as the base window size in CDP). As seen, our proposed CDP exhibits a 1.4% increase in average mAP relative to “Fixed”. This is because CDP offers better flexibility, allowing our model to tailor the attention based on multimodal inputs.

TABLE VI
EFFECT OF DIFFERENT BASE WINDOW SIZE IN CDP RELYING ON “ONE-PEACE” BACKBONE [1].

Base window size	0.5	0.6	0.7	0.8	0.9	Avg.
4	57.5	52.3	45.7	38.5	26.7	54.3
8	58.5	53.2	46.7	38.1	26.8	54.9
16	57.6	52.6	45.7	38.2	26.5	54.2
32	57.2	52.4	46.1	37.9	26.5	54.1
Full	57.4	52.2	45.4	37.1	25.7	53.8

Base Window Size. Tab. VI shows the effect of base window size W in CDP by increasing W from 4 to 32 based on ONE-PEACE features [1]. Compared with global cross-attention [12] in row #5 of Tab. VI (*i.e.*, “Full”), window-based attention in row #1 - #4 are more favored, due to high flexibility and capacity. The best results are observed with a window size of 8. We thus set the window size W to 8 in all the experiments by default. The performance degrades when the base window size W in CDP is either too large or too small, *e.g.*, increasing W from 8 to 32 leads to poorer performance (*i.e.*, from 58.5% to 57.2% in mAP@0.5). This might result from the increased difficulty in adjusting the attention area when the base window size is overly large.

Impact of Head Number H in CDP. We provide an additional ablation study on the head number H in Cross-modal Dynamic Perception (CDP) based on ONE-PEACE backbone [1]. As shown in Fig. 4, our model works best with $H = 4$. Both overly large and too small values of H result in degraded performance. Thus, we adopt $H = 4$ by default.

Impact of Weight α in Eq. 12. Fig. 5 depicts how different α influences average mAP based on ONE-PEACE features [1]. Average mAP rises when α increases and peaks at $\alpha = 0.1$. Beyond this value, the average mAP declines due to the excessive weight of \mathcal{L}_{LCC} relative to other loss components. Thus, we adopt $\alpha = 0.1$ by default.

TABLE VII
COMPARISON OF FLOPS AND PARAMETERS (SEE §IV-D) ACROSS DIFFERENT DAVE MODELS AND VARIANTS WITH BACKBONE ONE-PEACE [1]. “GB” IS GLOBAL CROSS-ATTENTION [12], [16]. “CDP” IS CROSS-MODAL DYNAMIC PERCEPTION. “LCC” IS LOCALITY-AWARE CORRESPONDENCE CORRECTION.

Method	FLOPs (G)	Parameters (M)	Avg.
UnAV	60.28	140.79	51.0
UniAV(STF)	32.83	186.00	51.7
base	18.26	71.35	37.0
base+GB	31.25	102.90	51.2
base+CDP	31.25	102.95	53.8
base+GB+LCC	31.45	103.68	53.8
Ours (base+LCC+CDP)	31.45	103.73	54.9

Parameter Analysis. In Tab. VII, we compare our methods with existing state-of-the-art methods and various variants regarding parameters and FLOPs. Tab. VII compares CDP (row #5) with global cross attention (row #4) used in previous methods [12], [16], showing CDP slightly increased the model’s parameters (0.05M) while bringing 2.6% average mAP improvement. LCC improves performance with only a minor and affordable increase in computational cost (0.2G FLOPs and 0.78M parameters), as observed in rows#5 and row #7 in Tab. VII. Note that compared to DAVE models (row #1-#2), our model has lower FLOPs and parameters, while achieving higher average mAP, *i.e.*, realizing more precise localization results.

E. Quality Analysis

Impact of Locality-aware Correspondence Correction. Fig. 3 visually illustrates Locality-aware Correspondence Correction (LCC, *c.f.* §III-C) enhances temporal feature discriminability by local cross-modal coherence constraint. The cross-similarity matrix (CSM) is calculated between audio and visual features from multimodal input encoding modules at different timestamps within the same video. Different from the original features (*i.e.*, without LCC module), “LCC features” are obtained by the model employing LCC module. We observe that LCC feature CSM exhibits a wider variety of similarities across different timestamps, demonstrating better feature discriminability. Besides, for all videos in UnAV-

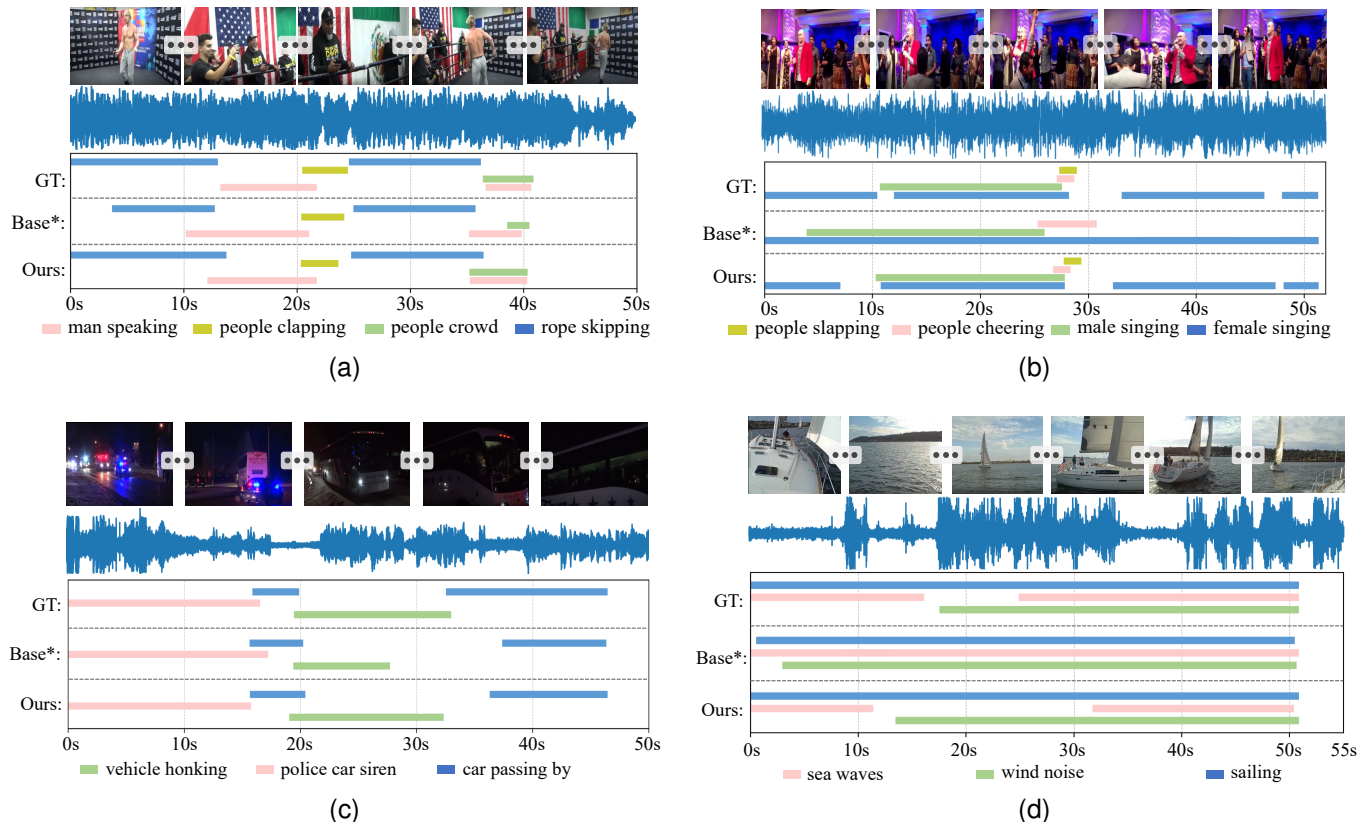


Fig. 6. **Qualitative detection results** on UnAV-100 test set. “GT”: ground truth. Our model displays boundaries exhibiting a high overlap with GT (See §IV-E).

100 [12] test split, we calculate the standard deviation of their CSM and then average them (*i.e.*, Mean of std). We find that “Mean of std” increases after adopting LCC module, suggesting greater temporal sensitivity in the features [68]. Concretely, the proposed LCC increases “Mean of std” by 0.269 (0.478 vs. 0.747) based on “I3D-VGGish” backbone [18], [19] and raises “Mean of std” by 0.187 (0.645 vs. 0.832) based on “ONE-PEACE” backbone, as shown in Fig. 3 (a) and (b).

Visualization of Localization Results. Fig. 6 presents the detection results with the backbone ONE-PEACE [1]. Our model achieves accurate temporal boundaries for each audio-visual event. As seen, our variant model Base* (*i.e.*, base model equipped with global cross-modal pyramid transformer [12], [16]) gets imprecise detection, *e.g.*, the “rope skipping” event in Fig. 6 (a) is incompletely detected by Base*, while the “sea waves” event in Fig. 6 (d) is over-completely detected by Base*. As shown in Fig. 6 (b), the “people slapping” event is omitted, and the “female singing” event is incorrectly localized throughout the entire video. In contrast, our model achieves more accurate temporal boundaries for each audio-visual event. This improvement is due to our model’s effective extraction of modality-shared information and its deliberate suppression of background noise.

V. CONCLUSION

In this paper, we present **LOCO**, a **L**ocality-aware cross-modal **C**orrespondence learning framework for **D**ense-localization **A**udio-**V**isual **E**vents (DAVE). LOCO makes use

of local cross-modal coherence to facilitate unimodal and cross-modal feature learning. The devised Locality-aware Correspondence Correction investigates cross-modal relations between intra- and inter-videos, guiding unimodal encoders towards modality-shared feature representation without extra annotations. To better integrate such audio and visual features, the insight from local continuity of audio-visual events in the video leads us to customize Cross-modal Dynamic Perception, which adaptively aggregates event-related features in a data-driven manner. Empirical results provide strong evidence to support the effectiveness of our LOCO. Our work opens a new avenue for DAVE from the perspective of learning audio-visual correspondence with the guidance of local cross-modal coherence, and we wish it to pave the way for multimodal scene understanding.

REFERENCES

- [1] P. Wang, S. Wang, J. Lin, S. Bai, X. Zhou, J. Zhou, X. Wang, and C. Zhou, “One-peace: Exploring one general representation model toward unlimited modalities,” *arXiv preprint arXiv:2305.11172*, 2023.
- [2] M. Chatterjee, N. Ahuja, and A. Cherian, “Learning audio-visual dynamics using scene graphs for audio source separation,” in *Annual Conference on Neural Information Processing Systems*, vol. 35, 2022, pp. 16 975–16 988.
- [3] D. J. Zhang, K. Li, Y. Wang, Y. Chen, S. Chandra, Y. Qiao, L. Liu, and M. Z. Shou, “Morphmlp: An efficient mlp-like backbone for spatial-temporal representation learning,” in *European Conference on Computer Vision*, 2022, pp. 230–248.
- [4] D. J. Zhang, J. Z. Wu, J.-W. Liu, R. Zhao, L. Ran, Y. Gu, D. Gao, and M. Z. Shou, “Show-1: Marrying pixel and latent diffusion models for text-to-video generation,” *arXiv preprint arXiv:2309.15818*, 2023.

- [5] D. Hu, Z. Wang, F. Nie, R. Wang, and X. Li, "Self-supervised learning for heterogeneous audiovisual scene analysis," *IEEE Transactions on Multimedia*, vol. 25, pp. 3534–3545, 2022.
- [6] S. Park, D. K. Han, and M. Elhilali, "Cross-referencing self-training network for sound event detection in audio mixtures," *IEEE Transactions on Multimedia*, vol. 25, pp. 4573–4585, 2022.
- [7] H. Qu, R. Yan, X. Shu, H. Gao, P. Huang, and G.-S. Xie, "Mvp-shot: Multi-velocity progressive-alignment framework for few-shot action recognition," *arXiv preprint arXiv:2405.02077*, 2024.
- [8] X. Wei, Y. Yao, H. Wang, and L. Zhou, "Perception-aware cross-modal signal reconstruction: From audio-haptic to visual," *IEEE Transactions on Multimedia*, vol. 25, pp. 5527–5538, 2022.
- [9] C. Liu, P. Li, H. Zhang, L. Li, Z. Huang, D. Wang, and X. Yu, "Bavs: bootstrapping audio-visual segmentation by integrating foundation knowledge," *IEEE Transactions on Multimedia*, 2024.
- [10] H. Han, Q. Zheng, M. Luo, K. Miao, F. Tian, and Y. Chen, "Noise-tolerant learning for audio-visual action recognition," *IEEE Transactions on Multimedia*, 2024.
- [11] Y. Tian, J. Shi, B. Li, Z. Duan, and C. Xu, "Audio-visual event localization in unconstrained videos," in *European Conference on Computer Vision*, 2018, pp. 247–263.
- [12] T. Geng, T. Wang, J. Duan, R. Cong, and F. Zheng, "Dense-localizing audio-visual events in untrimmed videos: A large-scale benchmark and baseline," in *IEEE Conference on Computer Vision and Pattern Recognition*, 2023, pp. 22942–22951.
- [13] H. Xu, R. Zeng, Q. Wu, M. Tan, and C. Gan, "Cross-modal relation-aware networks for audio-visual event localization," in *ACM International Conference on Multimedia*, 2020, pp. 3893–3901.
- [14] H. Xuan, Z. Zhang, S. Chen, J. Yang, and Y. Yan, "Cross-modal attention network for temporal inconsistent audio-visual event localization," in *AAAI Conference on Artificial Intelligence*, vol. 34, no. 01, 2020, pp. 279–286.
- [15] S. Ge, Z. Jiang, Y. Yin, C. Wang, Z. Cheng, and Q. Gu, "Learning event-specific localization preferences for audio-visual event localization," in *ACM International Conference on Multimedia*, 2023, pp. 3446–3454.
- [16] T. Geng, T. Wang, Y. Zhang, J. Duan, W. Guan, and F. Zheng, "Uniav: Unified audio-visual perception for multi-task video localization," *arXiv preprint arXiv:2404.03179*, 2024.
- [17] C.-L. Zhang, J. Wu, and Y. Li, "Actionformer: Localizing moments of actions with transformers," in *European Conference on Computer Vision*, 2022, pp. 492–510.
- [18] J. Carreira and A. Zisserman, "Quo vadis, action recognition? a new model and the kinetics dataset," in *IEEE Conference on Computer Vision and Pattern Recognition*, 2017, pp. 6299–6308.
- [19] S. Hershey, S. Chaudhuri, D. P. Ellis, J. F. Gemmeke, A. Jansen, R. C. Moore, M. Plakal, D. Platt, R. A. Saurous, B. Seybold *et al.*, "Cnn architectures for large-scale audio classification," in *IEEE International Conference on Acoustics, Speech and Signal Processing*, 2017, pp. 131–135.
- [20] Y.-B. Lin, Y.-J. Li, and Y.-C. F. Wang, "Dual-modality seq2seq network for audio-visual event localization," in *IEEE International Conference on Acoustics, Speech and Signal Processing*, 2019, pp. 2002–2006.
- [21] J. Yu, Y. Cheng, R.-W. Zhao, R. Feng, and Y. Zhang, "Mm-pyramid: Multimodal pyramid attentional network for audio-visual event localization and video parsing," in *ACM International Conference on Multimedia*, 2022, pp. 6241–6249.
- [22] J. Zhou, L. Zheng, Y. Zhong, S. Hao, and M. Wang, "Positive sample propagation along the audio-visual event line," in *IEEE Conference on Computer Vision and Pattern Recognition*, 2021, pp. 8436–8444.
- [23] S. Liu, W. Quan, C. Wang, Y. Liu, B. Liu, and D.-M. Yan, "Dense modality interaction network for audio-visual event localization," *IEEE Transactions on Multimedia*, vol. 25, pp. 2734–2748, 2022.
- [24] Y. Wu, L. Zhu, Y. Yan, and Y. Yang, "Dual attention matching for audio-visual event localization," in *International Conference on Computer Vision*, 2019, pp. 6292–6300.
- [25] Y. Xia and Z. Zhao, "Cross-modal background suppression for audio-visual event localization," in *IEEE Conference on Computer Vision and Pattern Recognition*, 2022, pp. 19989–19998.
- [26] J. Yu, Y. Cheng, and R. Feng, "Mpn: Multimodal parallel network for audio-visual event localization," in *IEEE International Conference on Multimedia and Expo*, 2021, pp. 1–6.
- [27] F. Feng, Y. Ming, N. Hu, H. Yu, and Y. Liu, "Css-net: A consistent segment selection network for audio-visual event localization," *IEEE Transactions on Multimedia*, 2023.
- [28] C. Xue, X. Zhong, M. Cai, H. Chen, and W. Wang, "Audio-visual event localization by learning spatial and semantic co-attention," *IEEE Transactions on Multimedia*, vol. 25, pp. 418–429, 2021.
- [29] Z. Liu, Y. Lin, Y. Cao, H. Hu, Y. Wei, Z. Zhang, S. Lin, and B. Guo, "Swin transformer: Hierarchical vision transformer using shifted windows," in *IEEE Conference on Computer Vision and Pattern Recognition*, 2021, pp. 10012–10022.
- [30] Z. Liu, H. Hu, Y. Lin, Z. Yao, Z. Xie, Y. Wei, J. Ning, Y. Cao, Z. Zhang, L. Dong *et al.*, "Swin transformer v2: Scaling up capacity and resolution," in *IEEE Conference on Computer Vision and Pattern Recognition*, 2022, pp. 12009–12019.
- [31] Q. Zhang, Y. Xu, J. Zhang, and D. Tao, "Vsa: Learning varied-size window attention in vision transformers," in *European Conference on Computer Vision*, 2022, pp. 466–483.
- [32] H. Qu, J. Wei, X. Shu, and W. Wang, "Learning clustering-based prototypes for compositional zero-shot learning," *arXiv preprint arXiv:2502.06501*, 2025.
- [33] I. Beltagy, M. E. Peters, and A. Cohan, "Longformer: The long-document transformer," *arXiv preprint arXiv:2004.05150*, 2020.
- [34] Q. Zhang, J. Zhang, Y. Xu, and D. Tao, "Vision transformer with quadrangle attention," *IEEE Transactions on Pattern Analysis and Machine Intelligence*, 2024.
- [35] S. Buch, V. Escorcia, C. Shen, B. Ghanem, and J. Carlos Niebles, "Sst: Single-stream temporal action proposals," in *IEEE Conference on Computer Vision and Pattern Recognition*, 2017, pp. 2911–2920.
- [36] F. C. Heilbron, J. C. Niebles, and B. Ghanem, "Fast temporal activity proposals for efficient detection of human actions in untrimmed videos," in *IEEE Conference on Computer Vision and Pattern Recognition*, 2016, pp. 1914–1923.
- [37] P. Zhao, L. Xie, C. Ju, Y. Zhang, Y. Wang, and Q. Tian, "Bottom-up temporal action localization with mutual regularization," in *European Conference on Computer Vision*, 2020, pp. 539–555.
- [38] Y. Liu, L. Ma, Y. Zhang, W. Liu, and S.-F. Chang, "Multi-granularity generator for temporal action proposal," in *IEEE Conference on Computer Vision and Pattern Recognition*, 2019, pp. 3604–3613.
- [39] N. Carion, F. Massa, G. Synnaeve, N. Usunier, A. Kirillov, and S. Zagoruyko, "End-to-end object detection with transformers," in *European Conference on Computer Vision*, 2020, pp. 213–229.
- [40] J. Kim, M. Lee, and J.-P. Heo, "Self-feedback detr for temporal action detection," in *International Conference on Computer Vision*, 2023, pp. 10286–10296.
- [41] J. Tan, J. Tang, L. Wang, and G. Wu, "Relaxed transformer decoders for direct action proposal generation," in *International Conference on Computer Vision*, 2021, pp. 13526–13535.
- [42] D. Shi, Y. Zhong, Q. Cao, J. Zhang, L. Ma, J. Li, and D. Tao, "React: Temporal action detection with relational queries," in *European Conference on Computer Vision*, 2022, pp. 105–121.
- [43] X. Liu, Q. Wang, Y. Hu, X. Tang, S. Zhang, S. Bai, and X. Bai, "End-to-end temporal action detection with transformer," *IEEE Transactions on Image Processing*, vol. 31, pp. 5427–5441, 2022.
- [44] D. Shi, Y. Zhong, Q. Cao, L. Ma, J. Li, and D. Tao, "Tridet: Temporal action detection with relative boundary modeling," in *IEEE Conference on Computer Vision and Pattern Recognition*, 2023, pp. 18857–18866.
- [45] H. Duan, Y. Xia, Z. Mingze, L. Tang, J. Zhu, and Z. Zhao, "Cross-modal prompts: Adapting large pre-trained models for audio-visual downstream tasks," in *Annual Conference on Neural Information Processing Systems*, vol. 36, 2024.
- [46] J. Wang, C. Li, A. Zheng, J. Tang, and B. Luo, "Looking and hearing into details: dual-enhanced siamese adversarial network for audio-visual matching," *IEEE Transactions on Multimedia*, vol. 25, pp. 7505–7516, 2022.
- [47] J. Zhou, D. Guo, and M. Wang, "Contrastive positive sample propagation along the audio-visual event line," *IEEE Transactions on Pattern Analysis and Machine Intelligence*, vol. 45, no. 6, pp. 7239–7257, 2022.
- [48] P. Wu, X. Liu, and J. Liu, "Weakly supervised audio-visual violence detection," *IEEE Transactions on Multimedia*, vol. 25, pp. 1674–1685, 2022.
- [49] J. Li, R. Selvaraju, A. Gotmare, S. Joty, C. Xiong, and S. C. H. Hoi, "Align before fuse: Vision and language representation learning with momentum distillation," in *Annual Conference on Neural Information Processing Systems*, vol. 34, 2021, pp. 9694–9705.
- [50] K. Cao, J. Ji, Z. Cao, C.-Y. Chang, and J. C. Niebles, "Few-shot video classification via temporal alignment," in *IEEE Conference on Computer Vision and Pattern Recognition*, 2020, pp. 10618–10627.
- [51] S. Kumar, S. Haresh, A. Ahmed, A. Konin, M. Z. Zia, and Q.-H. Tran, "Unsupervised action segmentation by joint representation learning and online clustering," in *IEEE Conference on Computer Vision and Pattern Recognition*, 2022, pp. 20174–20185.

- [52] K. D. Nguyen, Q.-H. Tran, K. Nguyen, B.-S. Hua, and R. Nguyen, "Inductive and transductive few-shot video classification via appearance and temporal alignments," in *European Conference on Computer Vision*, 2022, pp. 471–487.
- [53] Y. Xia, H. Huang, J. Zhu, and Z. Zhao, "Achieving cross modal generalization with multimodal unified representation," in *Annual Conference on Neural Information Processing Systems*, vol. 36, 2024.
- [54] J. Kim, H. Lee, K. Rho, J. Kim, and J. S. Chung, "Equiav: Leveraging equivariance for audio-visual contrastive learning," in *International Conference on Machine Learning*, 2024.
- [55] S. Jenni, A. Black, and J. Collomosse, "Audio-visual contrastive learning with temporal self-supervision," in *AAAI Conference on Artificial Intelligence*, vol. 37, no. 7, 2023, pp. 7996–8004.
- [56] R. Gao, T.-H. Oh, K. Grauman, and L. Torresani, "Listen to look: Action recognition by previewing audio," in *IEEE Conference on Computer Vision and Pattern Recognition*, 2020, pp. 10 457–10 467.
- [57] B. He, J. Wang, J. Qiu, T. Bui, A. Shrivastava, and Z. Wang, "Align and attend: Multimodal summarization with dual contrastive losses," in *IEEE Conference on Computer Vision and Pattern Recognition*, 2023, pp. 14 867–14 878.
- [58] B. Xu, N. Wang, T. Chen, and M. Li, "Empirical evaluation of rectified activations in convolutional network," *arXiv preprint arXiv:1505.00853*, 2015.
- [59] J. L. Ba, J. R. Kiros, and G. E. Hinton, "Layer normalization," *arXiv preprint arXiv:1607.06450*, 2016.
- [60] A. Vaswani, N. Shazeer, N. Parmar, J. Uszkoreit, L. Jones, A. N. Gomez, L. u. Kaiser, and I. Polosukhin, "Attention is all you need," in *Annual Conference on Neural Information Processing Systems*, vol. 30, 2017.
- [61] T.-Y. Lin, P. Goyal, R. Girshick, K. He, and P. Dollár, "Focal loss for dense object detection," in *International Conference on Computer Vision*, 2017, pp. 2980–2988.
- [62] H. Rezatofighi, N. Tsoi, J. Gwak, A. Sadeghian, I. Reid, and S. Savarese, "Generalized intersection over union: A metric and a loss for bounding box regression," in *IEEE Conference on Computer Vision and Pattern Recognition*, 2019, pp. 658–666.
- [63] N. Bodla, B. Singh, R. Chellappa, and L. S. Davis, "Soft-nms—improving object detection with one line of code," in *International Conference on Computer Vision*, 2017, pp. 5561–5569.
- [64] C. Zhao, A. K. Thabet, and B. Ghanem, "Video self-stitching graph network for temporal action localization," in *International Conference on Computer Vision*, 2021, pp. 13 658–13 667.
- [65] Z. Teed and J. Deng, "Raft: Recurrent all-pairs field transforms for optical flow," in *European Conference on Computer Vision*, 2020, pp. 402–419.
- [66] D. Kingma, "Adam: a method for stochastic optimization," in *International Conference on Learning Representations*, 2014.
- [67] Y. Gao, J. Liu, Z. Xu, J. Zhang, K. Li, R. Ji, and C. Shen, "Pyramidclip: Hierarchical feature alignment for vision-language model pretraining," in *Annual Conference on Neural Information Processing Systems*, vol. 35, 2022, pp. 35 959–35 970.
- [68] H. Kang, H. Kim, J. An, M. Cho, and S. J. Kim, "Soft-landing strategy for alleviating the task discrepancy problem in temporal action localization tasks," in *IEEE Conference on Computer Vision and Pattern Recognition*, 2023, pp. 6514–6523.



Ling Xing received the B.S. degree from Nanjing Forestry University, Nanjing, China. She is now a Ph.D. student in the School of Computer Science and Engineering at Nanjing University of Science and Technology. Her research interests include Video Understanding and Multimodal Learning.



Hongyu Qu received the B.S. degree from Nanjing Forestry University, Nanjing, China. He is now a Ph.D. student in the School of Computer Science and Engineering at Nanjing University of Science and Technology. His research interests include Human-centric AI and Data-efficient Learning.



Rui Yan received the Ph.D. degree at Intelligent Media Analysis Group (IMAG), Nanjing University of Science and Technology, China. He is currently an Assistant Researcher at the Department of Computer Science and Technology, Nanjing University, China. He was a research intern (part-time) at ByteDance from Jan. 2022 to Aug. 2022. He was a research intern (part-time) at Tencent from Sep. 2021 to Dec. 2021. He was a visiting researcher at the National University of Singapore (NUS) from Aug. 2021 to Aug. 2022. He was a research intern at HUAWEI NOAH'S ARK LAB from Dec. 2018 to Dec. 2019. His research mainly focuses on Complex Human Behavior Understanding and Video-Language Understanding. He has authored over 20 journal and conference papers in these areas, including IEEE TPAMI, IEEE TNNLS, IEEE TCSVT, CVPR, NeurIPS, ECCV, and ACM MM, etc.



Xiangbo Shu (Senior Member, IEEE) is currently a Professor in School of Computer Science and Engineering, Nanjing University of Science and Technology, China. Before that, he also worked as a visiting scholar in National University of Singapore, Singapore. His current research interests include Computer Vision, and Multimedia. He has authored over 80 journal and conference papers in these areas, including IEEE TPAMI, IEEE TNNLS, IEEE TIP, CVPR, ICCV, ECCV, ACM MM, etc. He has received the Best Student Paper Award in MMM 2016, and the Best Paper Runner-up in ACM MM 2015. He has served as the editorial boards of the IEEE TNNLS, and IEEE TCSVT. He is also the Member of ACM, the Senior Member of CCF, and the Senior Member of IEEE.



Jinhui Tang (Senior Member, IEEE) received the B.E. and Ph.D. degrees from the University of Science and Technology of China, Hefei, China, in 2003 and 2008, respectively. He is currently a Professor with the Nanjing University of Science and Technology, Nanjing, China. He has authored more than 200 articles in top-tier journals and conferences. His research interests include multimedia analysis and computer vision. Dr. Tang was a recipient of the Best Paper Awards in ACM MM 2007 and ACM MM Asia 2020, the Best Paper Runner-Up in ACM MM 2015. He has served as an Associate Editor for the IEEE TNNLS, IEEE TKDE, IEEE TMM, and IEEE TCSVT. He is a Fellow of IAPR.